

AKARI MIR slitless spectroscopic survey of galaxies at $z < 0.5$

Y. OHYAMA,¹

T. WADA, H. MATSUHARA, T. TAKAGI, M. MALKAN, T. GOTO, E. EGAMI, H.-M. LEE, M. IM, J.-H. KIM, C. PEARSON,
H. INAMI, S. OYABU, F. USUI, D. BURGARELLA, F. MAZYED, M. IMANISHI, W.-S. JEONG, T. MIYAJI, J. D'IAZ TELLO,
AND T. NAKAGAWA, S. SERJEANT, T. T. TAKEUCHI, Y. TOBA, G. J. WHITE, H. HANAMI, T. ISHIGAKI

¹*Academia Sinica, Institute of Astronomy and Astrophysics, 11F of Astronomy-Mathematics Building, AS/NTU, No. 1, Sec. 4, Roosevelt Rd., Taipei 10617, Taiwan, R.O.C.*

ABSTRACT

We aim to study star-forming galaxies by using a blind spectroscopic survey at mid-infrared (MIR) wavelengths to understand evolution of their star formation rate (SFR) and specific SFR (SFR per stellar mass) up to $z \sim 0.5$, by paying particular attention to their Polycyclic Aromatic Hydrocarbon (PAH) properties. We conducted a low-resolution ($R \approx 50$) slitless spectroscopic survey at 5–13 μm of 9 μm flux-selected sources ($\gtrsim 0.3$ mJy) around the North Ecliptic Pole with the Infrared Camera (IRC) onboard *AKARI*. We identified 48 PAH galaxies with PAH 6.2, 7.7, and 8.6 μm features at $z \lesssim 0.5$. The rest-frame optical-MIR spectral energy distributions (SEDs) based on CFHT and *AKARI*/IRC imaging are produced and analyzed in conjunction with the PAH spectroscopy. The rest-frame SEDs of all PAH galaxies have a universal shape with stellar and 7.7 μm (PAH) bumps, except that the PAH enhancement (luminosity ratio of the 7.7 μm PAH feature over the 3.5 μm stellar bump) significantly varies as a function of the PAH luminosities. We identified a PAH-enhanced population at $z \lesssim 0.35$, whose SEDs and luminosities are typical of luminous infrared galaxies. They show particularly larger PAH enhancement at high luminosity, implying that they are vigorous star-forming galaxies with elevated specific SFR. Our composite starburst model that combines a young and dusty starburst with a very old population can successfully reproduce most SED characteristics.

Keywords: galaxies: starburst – Infrared: galaxies – galaxies: evolution

1. INTRODUCTION

Deep mid-infrared (MIR) surveys have revealed numerous strongly star-forming galaxies at redshift $z \lesssim 2$. Their MIR fluxes are produced by a combination of continuum and Polycyclic Aromatic Hydrocarbon (PAH) emission features. The PAH features can dominate the total MIR flux, but are difficult to measure without spectroscopy. We have conducted MIR slitless spectroscopic survey toward North Ecliptic Pole (NEP), nicknamed *SPICY* (“slitless Spectroscopic survey of galaxies”) by using IRC onboard *AKARI*. This is a blind MIR spectroscopic survey for galaxy evolution study by using 9 μm -selected sample ($S_{9W} > 0.3$ mJy). This sensitivity corresponds roughly to > 0.3 mJy at 15 μm for our sample based on broad-band 15 $\mu\text{m}/9 \mu\text{m}$ (L_{15}/S_{9W}) color, reaching the strongly evolving population that *ISO* found at < 1 mJy at 15 μm (LW3) (e.g., Pearson et al. 2010). We aim to study star-forming galaxies to understand evolution of their star formation rate (SFR) and specific SFR (SFR per stellar mass) up to $z \sim 0.5$, by paying particular attention to their PAH properties.

Our target field, North Ecliptic Pole (NEP), is one of the ideal fields to study galaxy evolution at MIR (e.g., Matsuhara et al. 2006). The NEP is within *AKARI*'s continuous visibility zone, and multi-band photometric surveys with *AKARI*/IRC, NEP-Wide (Lee et al. 2009; Kim et al. 2012) and NEP-Deep (Wada et al. 2008; Takagi et al. 2012), have been conducted, covering 2–24 μm with 9 bands. Adding CFHT optical multi-band survey (Hwang et al. 2007), we have multi-band photometric information covering as wide as 0.3–18 μm with 13 bands in total. By further adding MIR spectroscopic survey, this study aims to provide spectroscopic basis to interpret photometric study results.

2. OBSERVATIONS, DATA, AND ANALYSIS

2.1. SPICY Spectroscopic Survey and Data

We performed low-resolution ($R \simeq 50$) IRC slit-less spectroscopic survey NEP around the NEP-Deep survey area. To achieve desired sensitivity (0.3 mJy at $9 \mu\text{m}$), we performed repeated (9–10 multi-pointing) observations at the same pointing coordinates. The data reduction was based on the standard way as implemented within so-called “IRC spectroscopy toolkit” (Ohyama et al. 2007), except for our own intermediate step to enable stacking multi-pointing spectra. This additional part is just to organize frames taken in different pointing datasets to be stacked at once, and the calibration was made entirely based on the original calibration data and algorithms within the toolkit. In this study, we focus on 5–13 μm spectra taken with the SG1 and SG2 grisms.

We performed simple spectral fitting with a model of four Lorentzian PAH (6.2, 7.7, 8.6, and $11.3 \mu\text{m}$) features over all detected sources at $> 0.3 \text{ mJy}$ at $9 \mu\text{m}$, and measured redshift and PAH luminosity for 48 galaxies (hereafter, the PAH galaxies) among all 171 detected sources. In this work, we discuss only the PAH galaxies.

2.2. Photometric Data

2.2.1. Compiling Photometric Data and Measuring Rest-Frame Properties

We compiled 14-band photometries from both the CFHT (Hwang et al. 2007) and AKARI NEP-Wide (Lee et al. 2009; Kim et al. 2012) surveys, and generated rest-frame SEDs by using the PAH redshift. During the course, we also measured photometric PAH luminosity (monochromatic luminosity at the peak of PAH $7.7 \mu\text{m}$ feature) and rest-frame colors.

The rest-frame SEDs show a universal two-bump structure: the OPT–NIR bump (or stellar bump) and the MIR bump peaking at $7.7 \mu\text{m}$ (or PAH bump). When normalized at either $3.5 \mu\text{m}$ (representative wavelength for the stellar bump among the IRC bands) and $7.7 \mu\text{m}$ (peak of the PAH bump), the rest-frame SEDs are almost identical within the sample. We then generated averaged rest-frame SEDs after grouping all PAH galaxies into three redshift bins ($z < 0.15$, $0.15 < z < 0.35$, and $z > 0.35$ for the nearby, mid- z , and higher- z sources, respectively) to explore SED evolution.

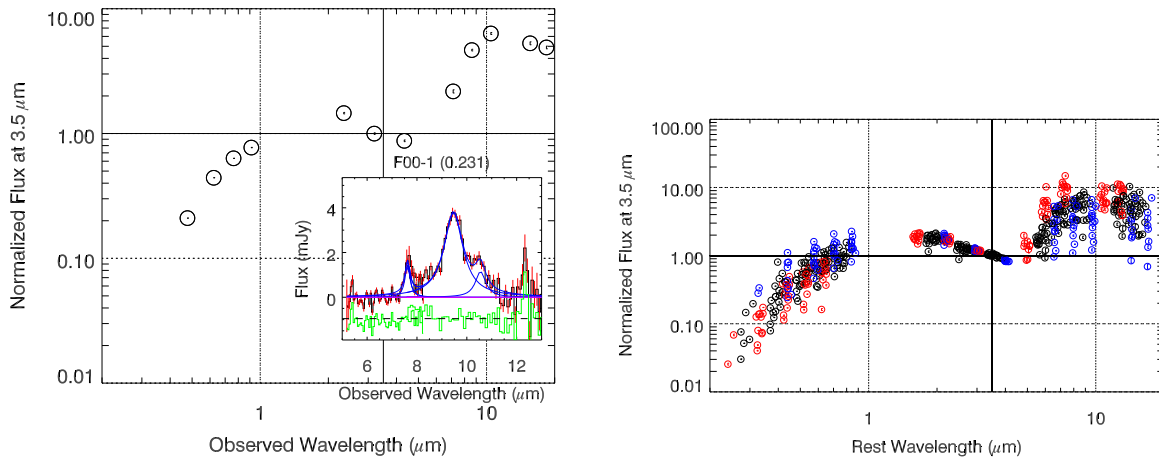


Figure 1. Left: An example of our basic dataset of the PAH galaxies. The 13-band CFHT (in SDSS system; u^* -band information is missing for this galaxy due to faintness)–IRC SED and *SPICY* spectrum (inset; observation (red), our PAH model-fit result (blue), and its residual (green)) are compared. Right: rest-frame SEDs of all PAH galaxies normalized at $3.5 \mu\text{m}$. The SEDs are shown in different colors for different redshift groups: blue, black, and red for the nearby, mid- z , and higher- z sources, respectively.

2.2.2. Predicting Observed Photometric Properties of Template/Model SEDs

To interpret the observed rest-frame SEDs, we compare the observations with the empirical templates of (Polletta et al. 2007; also known as the “SWIRE” template) and the theoretical SEDs of physical starburst evolutionary model (SBURT; Takagi et al. 2003). Note that the observed rest-frame SEDs are smoothed through the instrument’s filter responses ($R \sim 5$), and the same feature (e.g., complex PAH feature between 6–9 μm) is observed with different filters depending on the redshift. Therefore, we predicted the broad-band photometries of the template/model galaxies at different redshift, by mimicking the IRC observations and following the same data analysis procedure.

3. RESULTS

We compared the averaged rest-frame SEDs among the three redshift bins, and found that the PAH bump/stellar bump ratio (or rest $7.7 \mu\text{m}/3.5 \mu\text{m}$ luminosity ratio) is systematically larger at $z > 0.35$. This relative PAH enhancement over the stellar SED bump (hereafter, the PAH enhancement) shows a positive correlation with the PAH luminosity, i.e., the PAH enhancement is larger in galaxies with larger PAH luminosity. We then defined the PAH enhanced galaxies based on the rest $7.7 \mu\text{m}/3.5 \mu\text{m}$ luminosity ratio.

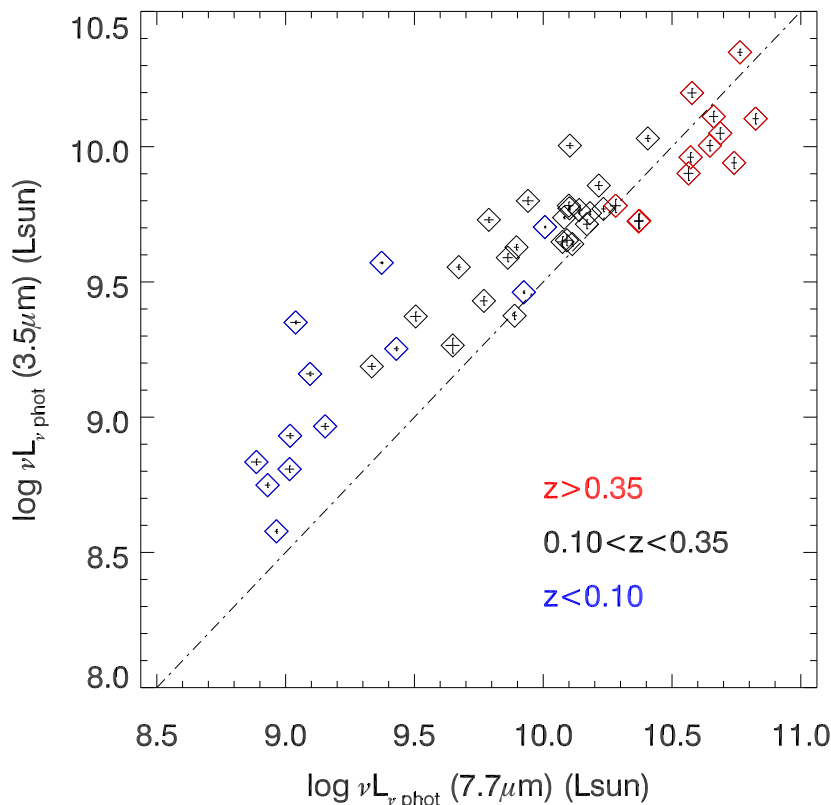


Figure 2. Comparison between the photometric monochromatic luminosities at $7.7 \mu\text{m}$, $\nu L_{\nu \text{ photo}}(7.7 \mu\text{m})$, and at $3.5 \mu\text{m}$, $\nu L_{\nu \text{ photo}}(3.5 \mu\text{m})$. The PAH galaxies are shown with one-sigma error bars in different colors for different redshift groups as in Figure 1. A diagonal dotted-broken line of a fixed PAH-to-stellar luminosity ratio is shown to identify PAH-enhanced population, on the lower right side of the line.

At $z < 0.35$, the observed rest-frame SEDs are consistent with either Sc or starburst (M82) SWIRE templates, and also with an older (400 Myr) starburst SBURT model. At $z > 0.35$, the SWIRE luminous infrared galaxy (LIRG) template (NGC 6090) reproduces the observations, including the enhanced PAH features. Note that the estimated IR (8–1000 μm) luminosity of the PAH galaxies from the PAH luminosity in this redshift is $L(\text{IR}) > 10^{11} L_{\odot}$, i.e., both their luminosities and SEDs are typical of LIRGs. On the other hand, we could not find appropriate SBURT models to match the observations, particularly the stellar SED bump: the observed stellar bump is typically as red as very old population, whereas the SBURT predicts much bluer one to enhance the PAH feature due to young starburst.

4. DISCUSSION

The PAH luminosity is almost proportional to SFR, and the PAH enhancement in terms of rest $7.7 \mu\text{m}/3.5 \mu\text{m}$ luminosity ratio is proportional to SFR per stellar mass, or specific SFR (sSFR). The positive correlation between them for the PAH galaxies indicates that sSFR is higher in galaxies with larger SFR. When compared to local blue star-forming galaxies forming so-called main sequence (Elbaz et al. 2007), most PAH enhanced population shows larger sSFR than the main sequence galaxies.

The PAH enhanced population seems to emerge at $z > 0.35$. Lack of PAH un-enhanced population at $z > 0.35$ is most likely due to selection effect, because such population tends to be fainter than our sensitivity limit at $9 \mu\text{m}$, where redshifted PAH $7.7 \mu\text{m}$ feature dominates the in-band flux of the *S9W* ($9 \mu\text{m}$) filter. However, lack of the PAH-enhanced population at $z < 0.35$ is not due to selection effect, because such sources are easier to be detected with the *S9W* filter. Nonetheless, we found 1 PAH-enhanced galaxy out of 25 PAH galaxies at $z < 0.35$, while 9 PAH-enhanced galaxy out of 13 PAH galaxies at $z > 0.35$. This difference is statistically significant with Fisher’s exact test.

The rest-frame SEDs of the PAH enhanced population can not be explained by simple SBURT SEDs in a consistent way across all OPT–NIR–MIR wavelengths. We examined if a two-component composite SED that combines SEDs of very old (SWIRE 13 Gyr old Elliptical) and very young dusty (70 Myr SBURT starburst with small compactness parameter) populations. We found a reasonable composite that can reproduce the observations, where the young starburst is so dusty and extinct in both OPT and NIR while contributing at MIR, whereas the old population dominates the OPT–NIR SED. This composite is actually very similar to the SWIRE LIRG template.

5. SUMMARY

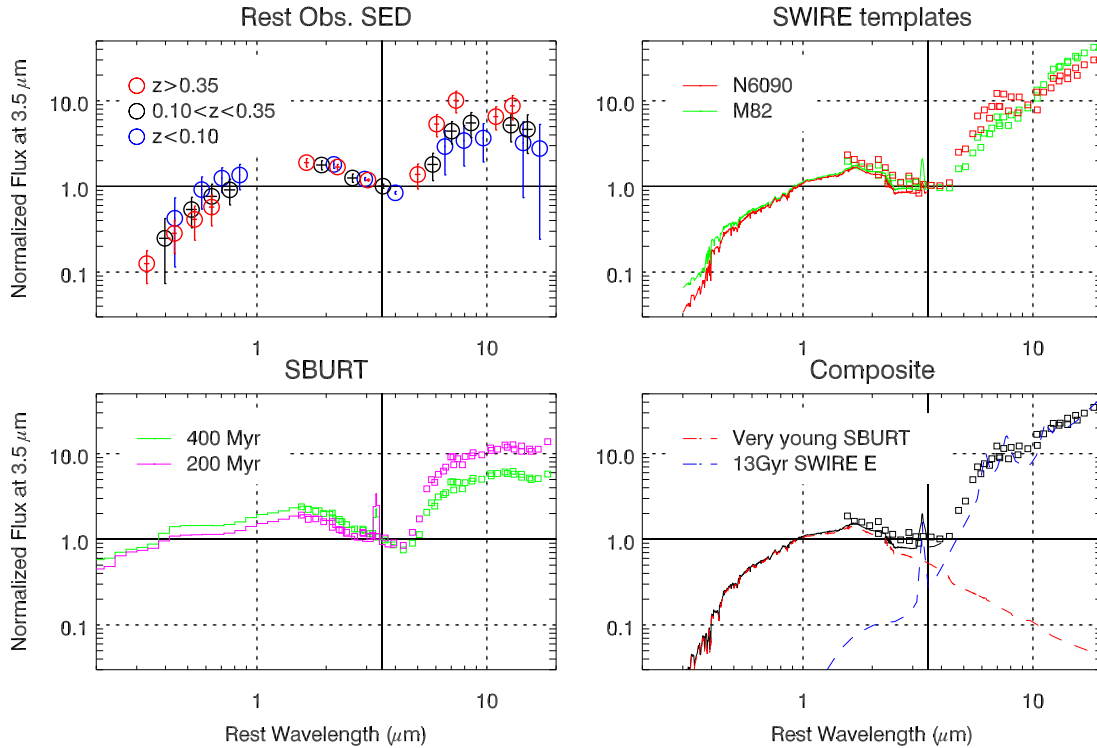


Figure 3. Comparison of the rest-frame $3.5 \mu\text{m}$ -normalized SEDs of the PAH galaxies and the templates/models. Top left: the averaged observed SEDs of Figure 1. The median SED is made for each redshift bin. The error bars are for one-sigma scatter from the median. Top right: the SWIRE SED templates M82 (green) and NGC 6090 (red). Bottom left: the SBURT SEDs with the burst age of 400 Myr and 200 Myr in green and magenta, respectively. Bottom right: two-component composite SED (black) that combines the SWIRE E (13 Gyr old) template (red broken line) and a very young (70 Myr) and compact SBURT SED (blue broken line).

We performed blind MIR spectroscopic survey toward NEP, nicknamed *SPICY*, by utilizing a unique capability of the IRC instrument onboard *AKARI*, and obtained $5\text{--}13 \mu\text{m}$ spectra of flux-limited ($> 0.3 \text{ mJy}$) sample at $9 \mu\text{m}$ up to $z \approx 0.5$. We also studied 14-band OPT–NIR–MIR ($0.3\text{--}18 \mu\text{m}$) SEDs of the *SPICY* sample based on both *AKARI* NEP-Wide and CFHT optical surveys, and analyzed them in conjunction with the PAH spectroscopy. We studied star-forming galaxies to understand evolution of their SFR and sSFR, paying particular attention to their PAH properties.

The PAH galaxies show universal rest-frame OPT–NIR–MIR SED shape, but relative strength of the PAH bump with respect to the stellar bump is systematically larger for larger PAH luminosities. At $z > 0.35$, most PAH galaxies show larger rest $7.7 \mu\text{m}/3.5 \mu\text{m}$ luminosity ratio than those at $z < 0.35$. We then defined the PAH-enhanced population based on this luminosity ratio. We found that they show larger sSFR than local main sequence galaxies. They are classified as LIRGs in terms of total infrared luminosity estimated based on the PAH luminosity.

We found that the SEDs of the PAH-enhanced population can be reproduced by both the SWIRE LIRG template and a composite SED made of a very young starburst on top of a very old population. Here, the composite is made of a very young dusty SBURT starburst and a SWIRE Elliptical galaxy to constitute the stellar and the MIR bumps, respectively.

ACKNOWLEDGMENTS

This research is based on observations with *AKARI*, a JAXA project with the participation of ESA.

REFERENCES

- Elbaz, D., Daddi, E., Le Borgne, D., et al. 2007, *A&A*, 468, 33
Hwang, N., Lee, M. G., Lee, H. M., et al. 2007, *ApJS*, 172, 583
Kim, S. J., Lee, H. M., Matsuhara, H., et al. 2012, *A&A*, 548, A29
Lee, H. M., Kim, S. J., Im, M., et al. 2009, *PASJ*, 61, 375
Matsuhara, H., Wada, T., Matsuura, S., et al. 2006, *PASJ*, 58, 673
Ohya, Y., Onaka, T., Matsuhara, H., et al. 2007, *PASJ*, 59, 411
Pearson, C. P., Oyabu, S., Wada, T., et al. 2010, *A&A*, 514, A8
Polletta, M., Tajer, M., Maraschi, L., et al. 2007, *ApJ*, 663, 81
Takagi, T., Arimoto, N., & Hanami, H. 2003, *MNRAS*, 340, 813
Takagi, T., Matsuhara, H., Goto, T., et al. 2012, *A&A*, 537, A24
Wada, T., Matsuhara, H., Oyabu, S., et al. 2008, *PASJ*, 60, 517